HHS Public Access

Author manuscript

Phys Med Biol. Author manuscript; available in PMC 2019 January 22.

Published in final edited form as:

Phys Med Biol. ; 63(3): 035002. doi:10.1088/1361-6560/aaa30d.

Focused Ultrasound-Facilitated Brain Drug Delivery Using Optimized Nanodroplets: Vaporization Efficiency Dictates Large Molecular Delivery

Shih-Ying Wu[a], **Samantha M. Fix**[b], **Christopher Arena**[c], **Cherry C. Chen**[a], **Wenlan Zheng**[a], **Oluyemi O. Olumolade**[a], **Virginie Papadopoulou**[c], **Anthony Novell**[c], **Paul A. Dayton**[c], and **Elisa E. Konofagou**[a,d]

[a]Department of Biomedical Engineering, Columbia University, New York, NY 10027

[b]Eshelman School of Pharmacy, University of North Carolina, Chapel Hill, NC 27599

[c]Joint Department of Biomedical Engineering, University of North Carolina and North Carolina State University, Chapel Hill, NC 27599

[d]Department of Radiology, Columbia University, New York, NY 10032

Abstract

Focused ultrasound with nanodroplets could facilitate localized drug delivery after vaporization with potentially improved *in vivo* stability, drug payload, and minimal interference outside of the focal zone compared with microbubbles. While the feasibility of blood-brain barrier (BBB) opening using nanodroplets has been previously reported, characterization of the associated delivery has not been achieved. It was hypothesized that the outcome of drug delivery was associated with the droplet's sensitivity to acoustic energy, and can be modulated with the boiling point of the liquid core. Therefore, in this study, octafluoropropane (OFP) and decafluorobutane (DFB) nanodroplets were used both *in vitro* for assessing their relative vaporization efficiency with high-speed microscopy, and *in vivo* for delivering molecules with a size relevant to proteins (40-kDa dextran) to the murine brain. It was found that at low pressures (300–450 kPa), OFP droplets vaporized into a greater number of microbubbles compared to DFB droplets at higher pressures (750–900 kPa) in the *in vitro* study. In the *in vivo* study, successful delivery was achieved with OFP droplets at 300 kPa and 450kPa without evidence of cavitation damage using ¼ dosage, compared to DFB droplets at 900 kPa where histology indicated tissue damage due to inertial cavitation. In conclusion, the vaporization efficiency of nanodroplets positively impacted the amount of molecules delivered to the brain. The OFP droplets due to the higher vaporization efficiency served as better acoustic agents to deliver large molecules efficiently to the brain compared with the DFB droplets.

Keywords

ultrasound; blood-brain barrier; drug delivery; nanodroplet; cavitation

Correspondence to: Elisa E. Konofagou.

1. Introduction

The blood-brain barrier (BBB) is a highly selective barrier that blocks most of the therapeutic agents from entering the brain parenchyma (Banks, 2016). Focused ultrasound (FUS) with microbubbles could open the BBB and facilitate drug delivery (Konofagou, 2012; Liu et al., 2014; Leinenga *et al.*, 2016). To date, several molecules have been successfully delivered with this technique including magnetic resonance contrast agents, various sizes of dextran, nanoparticles, chemotherapeutic agents, neurotrophic factors, genes, etc (Timbie *et al.*, 2015). However, the delivery was found to be more contained and thus difficult for largermolecules (Choi *et al.*, 2010; Chen and Konofagou, 2014). Successful and sufficient delivery of large molecules was often accompanied by undesirable tissue damage such as hemorrhage (Chen and Konofagou, 2014; Chen *et al.*, 2014), which hinders the treatment of delivering promising therapeutics such as proteins, antibodies, and neurotrophic factors for neurodegenerative diseases or brain tumors (Liu *et al.*, 2016a; Baseri *et al.*, 2012; Kinoshita *et al.*, 2006b, a). Moreover, bubble shielding effects (clusters of bubbles in the pre-focal area scattering acoustic waves) caused either the failure of BBB opening (Marquet *et al.*, 2011) or undesired BBB opening in the pre-focal area in large animals (Wu *et al.*, 2016).

Nanodroplets, as liquid-state phase-change contrast agents, hold great potential to solve these problems after vaporization into microbubbles with sufficient acoustic energy only in the center of focal area (Kripfgans *et al.*, 2000; Sheeran *et al.*, 2011b; Mountford *et al.*, 2015), which generates highly concentrated mechanical stress in the targeted vessels. They have been used in therapeutic applications such as BBB opening (Chen *et al.*, 2013a), drug delivery (Zhou, 2015), thermal ablation (Moyer *et al.*, 2015; Phillips *et al.*, 2013; Kopechek *et al.*, 2014), or embolization with larger droplets (Samuel *et al.*, 2012; Kripfgans *et al.*, 2002) as well as contrast agents for imaging (Dayton *et al.*, 2006; Matsunaga *et al.*, 2012; Porter *et al.*, 2016). Not only are they characterized by the high echogenicity of conventional microbubble contrast agents post-vaporization, they also exhibit several advantages over bubbles prior to vaporization. First, they may have better in-vivo stability than microbubbles as they are not subject to rapid deflation due to gas diffusion in the bloodstream (Sheeran *et al.*, 2015). Second, the pressure threshold required for vaporization into microbubbles provides a localized delivery method without microbubble interference outside of the focal zone for BBB opening and drug delivery. Third, their capacity to carry high payloads demonstrates significant improvement on targeted treatment and imaging (Wang *et al.*, 2013; Liu *et al.*, 2016b; Rapoport *et al.*, 2011).

The current challenge associated with nanodroplets for brain drug delivery is the low amount of delivery even with small molecules at relatively high pressures compared to using microbubbles. In our first attempt of using decafluorobutane (DFB) nanodroplets for drug delivery to the brain, successful BBB opening was achieved with a significantly lower amount of small molecules (3 kDa dextran) delivered compared to microbubbles (Chen *et al.*, 2013a). We hypothesize that it was due to a small amount of bubbles generated from DFB droplet vaporization, and that the amount and size of drug delivered was associated with the droplet's sensitivity to acoustic energy. Since the sensitivity or the vaporization efficiency of nanodroplets can be modulated by the boiling point of the perfluorocarbon

(PFC) cores (Sheeran *et al.*, 2012), in this study, the relationship of droplet vaporization efficiency (the sensitivity to acoustic energy represented by the vaporization threshold and the relative number of bubbles generated from droplet solution in the focal zone) and the drug delivery efficiency was investigated using nanodroplets of different boiling points in the condensed cores.

The objective of this study is to characterize nanodroplets for delivering large molecules to the brain. Lipid-shelled nanodroplets were first customized for delivering large molecules to the brain via investigating the relationship of drug delivery and the nanodroplet vaporization efficiency. Octafluoropropane (OFP, boiling point: −36.7 °C) nanodroplets and decafluorobutane (DFB, boiling point: −1.7 °C) nanodroplets were used separately in the *in vitro* high-speed microscopy and *in vivo* BBB opening studies for comparison. *In vitro* high-speed microscopy was used to investigate the vaporization threshold and efficiency. Then, *in vivo* BBB opening with delivery of 40-kDa dextran (size relevant to proteins) was performed in mice, with acoustic signals monitored during sonication in order to reveal the physical mechanism of cavitation to the drug delivery after droplet vaporization. The delivery efficiency and the potential to cause cavitation-induced bioeffects were assessed with fluorescence microscopy and histological staining, respectively.

2. Materials and methods

2.1 Nanodroplet generation and characterization

Perfluorocarbon (PFC) droplets containing condensed gases of different boiling points (octafluoropropane or OFP: −36.7 °C, decafluorobutane or DFB: −1.7 °C) (FluoroMed, Round Rock, TX, USA) were fabricated as previously described (Sheeran *et al.*, 2011a; Sheeran *et al.*, 2012). Briefly, 1,2-distearoyl-sn-glycero-3-phosphocholine (DSPC) and 1,2-distearoyl-sn-glycero-3-phosphoethanolamine-N-[methoxy(polyethylene glycol)2000] (DSPE-PEG2000) (Avanti Polar Lipids, Alabaster, AL, USA) were combined at a 9:1 molar ratio and dissolved in a phosphate-buffered saline (PBS)-based excipient solution containing 15% (v/v) propylene glycol and 5% (v/v) glycerol for a final lipid concentration of 1.0 mg/mL. The resultant lipid solution (1.5 mL) was added to 3 mL glass vials, and the headspace air was exchanged with OFP or DFB gas. Microbubbles were formed by vigorous shaking of the lipid-filled vials using a Vialmix mixer (Bristol-Myers-Squibb, New York, NY, USA). The nanodroplets were then generated via microbubble condensation under reduced temperature and increased ambient pressure, as per our previously published protocol (Sheeran *et al.*, 2012). Briefly, vials of microbubbles were immersed in an isopropanol/CO_2 bath maintained between −8°C and −13°C for approximately 2 minutes. The vials were then attached to an adjustable pressure source, and the headspace pressure was increased until condensation was observed.

The size distribution and concentration of nanodroplets were measured using a Malvern NanoSight NS500 (Malvern, Worcestershire, UK). This instrument measures nanoparticle size based on their Brownian motion and is able to detect particles between 30 and 2000 nm. Number-weighted size distributions and particle concentrations were measured using three vials of OFP- and DFB-filled nanodroplets. To assess the amount of droplets in the micron range or spontaneously vaporized microbubbles, droplet formulations were analyzed using

an Accusizer (Accusizer 780AD, Particle Sizing Systems, USA) and Multisizer III particle counter (Beckman Coulter Inc., USA) as well. Similarly, the size distribution and concentration of the precursor microbubble were characterized using a Multisizer III particle counter.

2.2 *In vitro* experiment for acoustic droplet vaporization

Droplet vaporization characteristics including the vaporization threshold and relative vaporization efficiency (i.e., relative number of bubbles generated from nanodroplets in the measurement field of view with given acoustic parameters) were investigated *in vitro* using a previously described high-speed optical microscopy setup (Chen *et al.*, 2013a). Briefly, an inverted microscope with a 100× objective (Olympus IX71; Center Valley, PA, USA) interfaced with a high-speed camera (1000 fps, FastCam SA1.1; Photron Inc., San Diego, CA, USA) was mounted on a water bath filled with degassed water at 37°C. A spherically focused transducer (A305S; Panametrics, Inc., Waltham, MA, USA) with a focal size of 0.75 mm laterally and 2 mm axially was used to activate the droplets by sending a single sinusoidal pulse of 1.5 MHz, 50 cycles at 150–900 kPa per video driven by an arbitrary waveform generator (AWG 2021; Tektronix, Inc., Beaverton, OR, USA) through a radiofrequency amplifier (A500; ENI, Rochester, NY, USA). Short pulses were used in order to better visualize vaporization with lower interference of stable and inertial cavitation after vaporization.

Before the experiments, the transducer focus was calibrated and aligned with the optical focus using a calibrated needle hydrophone (HNA-0400; ONDA Corp., Sunnyvale, CA, USA). The hydrophone at the center of the focus was then replaced with a nearly optically and acoustically transparent microcellulose tube (200 μm in diameter, Spectrum Laboratories INC., Greensboro, NC, USA), which was aligned with the microscope field of view using a micropositioner (MMO-203; Narishige Group, East Meadow, NY, USA). Nanodroplets (both OFP and DFB) were diluted by 50% in PBS and pumped through the microcellulose tube for visualization before sonication. At each experiment, the droplet solution was static in the tube while a trigger pulse was transmitted from the waveform generator to the high-speed camera to allow synchronized video recording of the droplet vaporization events after sonication together with 10 frames right before sonication in the buffer memory.

After the experiments, the videos for the nanodroplet vaporization activity were analyzed offline to determine the pressure threshold required for vaporization, and to count the number of bubbles generated in the microscope field of view (an estimate of vaporization efficiency). Bubbles were counted using a customized image processing program in MATLAB (Mathworks Inc., Natick, MA, USA) based on the Hough transform for circle pattern recognition (Supplementary Fig. 1) (Davies, 1988; Li *et al.*, 1986). The lighting in the setup allowed for good contrast between the background and the formed bubbles, and the use of the Hough transform for circle recognitions allowed for accurate identification of bubbles since the principal radius component was chosen through an ordered voting process. Bubbles vaporized within a finite width slice around the plane of focus of the camera were counted, while those completely out of focus become part of the background (fuzzy dark

shadows) and were therefore not counted. Since this plane remained the same between OFP and DFB experiments, our quantification yielded a relative vaporization efficiency between OFP and DFB nanodroplets activated *in vitro*.

Ten videos were recorded in order to account for variability with each parameter setting: 1) intra-vial vaporization variability – five videos of vaporization were captured using a single vial of nanodroplets and the tube was flushed between captures to ensure a fresh sample was introduced; 2) inter-vial variability – an additional five vaporization events were recorded using an independent vial of droplets to observe any batch-to-batch variability. The inter-vial standard deviation was smaller than the intra-vial standard deviation (Supplementary Fig. 2), showing that the stochastic nature of the vaporization process outweighs any vaporization differences due to solution preparation.

2.3 *In vivo* experiments for BBB opening

All animal studies were conducted in accordance with the National Institutes of Health Guidelines for animal research, and all procedures were approved by the Columbia University Institutional Animal Care and Use Committee. Male C57BL/6 mice (Harlan Laboratories, Indianapolis, IN, USA) weighing 20–25 g were randomly divided into each experimental group as listed in Table 1. Before sonication, each mouse was anesthetized using a 1–2% isoflurane-oxygen mixture (SurgiVet; Smiths Medical PM, Norwell, MA, USA) and its scalp fur was removed with an electric clipper and a depilatory cream. The animal body temperature was maintained throughout the experiment using a heating pad. A modified 27G×½ butterfly catheter (Terumo Medical, Somerset, NJ, USA) was inserted into the tail vein for injection of the nanodroplets mixed with the fluorescently-tagged dextran in cohort 1 and 2 (molecular weight: 40-kDa, Stoke-Einstein hydrodynamic diameter: 10 nm, fluorochrome: Texas Red), a model drug with sizes comparable to proteins. The purchased dextran (Life Technologies, Carlsbad, CA, USA) was dissolved to a weight concentration of 40 mg/mL using sterile saline (Fisher Scientific, Pittsburgh, PA, USA), and then 50 μL of the dextran solution was co-administered with either OFP, DFB droplets (25 μL of OFP droplets in cohort 1 or 100 μL of DFB droplets in cohort 2 diluted with 50 μL of sterile saline) or microbubbles (30 μL with a concentration of 8×10^8 particles/mL). Note that the droplet emulsions stored at −80 °C were thawed at 4 °C immediately before the injection in order to maintain the stability at low temperature, and the solution appeared to be translucent in contrast to the milky microbubble solution.

The experimental setup and procedure were described elsewhere (Wu *et al.*, 2015). A single-element, ring-shaped, 1.5 MHz FUS transducer (Imasonic, Besancon, France) was calibrated with the hydrophone (−6 dB focal size: 1.3 mm laterally and 10.6 mm axially) and driven by a function generator (33220A; Agilent Technologies, Palo Alto, CA, USA) through a 50-dB power amplifier (325LA; E&I, Rochester, NY, USA. A pulse-echo transducer (center frequency: 10 MHz, focal length: 60 mm; Olympus NDT, Waltham, MA, USA) confocally and coaxially aligned with the FUS transducer was used for both targeting and passive cavitation detection (PCD) purposes. During the targeting procedure, the pulse-echo transducer was driven by a pulser receiver (Model 5800; Parametrics-NDT, MA, USA) in transmit and receive mode; while for PCD during sonication, it was operated in receive-only

mode with 20 dB of amplification. The signal was digitized with a 50-MHz sampling rate (CompuScope 1422, 14 bits; Gage Applied Technologies, Lachine, QC, Canada) and saved for offline processing.

FUS (pulse length: 10000 cycles or 6.7 ms, pulse repetition frequency (PRF): 5 Hz, duration: 5 min) at acoustic pressures ranging between 150 and 900 kPa (derated peak-rarefactional pressure after accounting for 18.1% loss through the murine skull (Choi *et al.*, 2007)) was applied transcranially to the targeted left hippocampus of the mouse brain while the right hippocampus served as the control without FUS. After the FUS transducer was aligned with the targeted region following the procedure described previously (Choi *et al.*, 2007), it was sonicated for 30 s before injecting acoustic agents as a baseline control for PCD. Then the prepared nanodroplet or microbubble solution was injected as a bolus intravenously followed by the 5-min sonication initiated within 5 s of injection. In addition, the sham cohort injected with OFP nanodroplets and dextran without sonication served as the basis for comparison of successful drug delivery in the fluorescence imaging analysis (see Section 2.4).

A 1-h period was allowed after sonication to enable the fluorescent model drugs to circulate throughout the vasculature and to diffuse into the brain parenchyma. At the end of the allotted time, the animal was sacrificed by transcardial perfusion using 30 mL phosphate buffer saline (PBS) for 5 min followed by 60 mL 4% paraformaldehyde for 8 min through the ventricular catheter connected with an infusion pump, and the blood was pumped out from the pierced right atrium. The mouse brain was extracted from the skull, post-fixed in 4% paraformaldehyde overnight before sectioning for either fluorescence imaging or hematoxylin or eosin (H&E) staining in order to evaluate drug delivery efficiency and bioeffects, respectively.

2.4 Fluorescence imaging and analysis

The post-fixed brains for drug delivery efficiency analysis were cryo-protected (30% of sucrose for 48 h) and then sectioned horizontally in transverse planes using a cryostat (Leica RM2255; Leica Microsystems Inc., Buffalo, IL, USA) into 60-μm slices covering the hippocampi as described previously (Wu *et al.*, 2015). The 60-μm frozen sections were used to quantify the fluorescence intensity increase (sum of fluorescence enhancement in the sonicated hippocampus) as well as the area of BBB opening (ratio of the area with successful dextran delivered in the sonicated hippocampus through BBB opening to the area in the contralateral hippocampus).

The epi-fluorescence images of the brain sections were captured for quantifying the fluorescence enhancement using an Olympus DP30BW digital camera mounted on an up-right Olympus BX61 microscope (Melville, NY, USA). Briefly, a section representing the ventral-dorsal mid-plane, as determined by anatomical landmarks of the hippocampi, was first selected, and eight adjacent sections were then selected on the ventral and the dorsal side of the mid-plane. The left (sonicated) and the right (unsonicated control) hippocampus were manually delineated using MATLAB (Mathworks Inc., Natick, MA, USA), and the fluorescence intensity increase as well as the BBB opening area were calculated (Chen *et al.*, 2014). The fluorescence images for all animals were normalized and thresholded by dividing

by the background intensity defined as spatial average of the region without the tissue adding three times its standard deviation. The area of the BBB opening in the sonicated hippocampus was calculated as a percentage of the BBB opening area over the unsonicated hippocampus over nine sectioned slices. The fluorescence intensity increase was quantified as the sum of fluorescence intensity in the sonicated hippocampus subtracting the sum of the unsonicated hippocampus. For each brain, the reported fluorescence intensity increase was thus equal to the sum of all nine sections. The BBB opening area (intensity > background) denoted the percentage normalized to the size of the hippocampus assuming the same hippocampus volume on the contra- and ipsi-lateral side. A successful dextran delivery for an individual brain was concluded if both the fluorescence intensity increase and the BBB opening area were higher by three times the standard deviation relative to the average of the corresponding sham cohort.

2.5 Cavitation dose quantification for PCD

Three types of cavitation dose (SCD_h, stable cavitation dose using harmonics; SCD_u, stable cavitation dose using ultraharmonics; ICD, inertial cavitation dose) were quantified (Wu et al., 2015; Wu *et al.*, 2014). First, the PCD signal of each pulse was converted into the frequency domain using fast Fourier transform in MATLAB (Mathworks Inc., Natick, MA, USA). Second, after taking the root mean square (rms) of the voltage spectral amplitude, the harmonic signal (n*f; n = 3, 4, 5, 6; f = 1.5 MHz; maximum amplitude within a bandwidth of 20 kHz around the harmonic frequency), ultraharmonic signal (n*f+0.5*f; n = 2, 3, 4, 5; f = 1.5 MHz; maximum amplitude within a bandwidth of 20 kHz around the ultraharmonic frequency), and the broadband signal in 3–9 MHz between them (applying a comb filter to suppress the harmonic and ultraharmonic signal with rejection bandwidths of 350 kHz and 100 kHz, respectively) (Wu *et al.*, 2015) were separately extracted. Third, the mean harmonic, ultraharmonic, and broadband signal were taken for each pulse and summed up over all pulses received during sonication to acquire SCD_h, SCD_u, and ICD, respectively. Lastly, the differential cavitation doses were computed by subtracting the normalized baseline cavitation doses (30s of sonication before droplet or microbubble injection). The cavitation doses reported in this study denote the differential cavitation doses.

2.6 Histological evaluation

The histological examination via hematoxylin and eosin (H&E) staining was performed for bioeffect assessment of both left and right hippocampi 1 h after sonication in cohorts with successful dextran delivery (N=3 in each cohort). The bright-field, stained images were captured by an Olympus DP25 digital camera mounted on the same microscope (Section 2.4), which can be used to identify damaged neurons (dark neurons showing shrunken and triangulated cell bodies) and red blood cell extravasations (hemorrhage) (Baseri *et al.*, 2010). Following the post-fixation process (Section 2.3), the brains for bioeffect assessment were paraffin embedded and then sectioned horizontally using a cryostat into 6-μm slices with 180-μm gaps covering the hippocampi. This histological examination was double-blinded, i.e., without knowledge of the droplet type or the sonicated side.

2.7 Statistical analysis

The in vitro droplet vaporization efficiency and the in vivo fluorescence increase after BBB opening was compared using one-way ANOVA with Newman-Keuls multiple comparison test for all groups. The cavitation doses were compared between groups with and without nanodroplets using the two-tailed, nonparametric Mann-Whitney test. The p-values were considered statistically significant if lower than 0.05, where * represents $p < 0.05$, ** for $p < 0.01$, *** for $p < 0.001$, and ns for $p > 0.05$. The analysis was performed in GraphPad Prism (La Jolla, CA, USA). The error bar in all figures represented standard error of the mean.

3. Results

3.1 Nanodroplet vaporization in vitro

Three different vials of each type of droplets were taken for measuring the size distribution and the concentration (Fig. 1). The mean, median, and mode size of the OFP droplets were 171.2±2.7 nm (mean ± standard deviation), 153.3±3.0 nm, and 109.1±5.6 nm, respectively; those for the DFB droplets were 182.5±3.4 nm, 163.4±0.7 nm, and 145.1±7.0 nm, respectively (Fig. 1). The average concentration was 2.8×10^{11} particles/mL and 1.3×10^{11} particles/mL for OFP and DFB droplets, respectively. Therefore, after a 50% dilution, the droplet concentration in the in vitro setup was 1.4×10^{11} particles/mL and 6.3×10^{10} particles/mL for OFP and DFB droplets, respectively. The high concentration was intended so as to capture vaporization events within the narrow field of view in the microscope. For micron-sized particles (within 0.5 – 500 μm) such as droplets and bubbles vaporized during the handling procedure, the concentrations were $2.51\times10^{8} \pm 5.69\times10^{7}$ particles/ml and $2.06\times10^{8} \pm 3.08\times10^{7}$ particles/ml for OFP and DFB droplets, respectively (Supplementary Fig. 3). This corresponds to 0.09% and 0.16% of the total droplet population for OFP and DFB droplets, respectively.

In order to investigate the acoustic vaporization threshold and the vaporization efficiency for the droplets, high-speed optical microscopy was used in the *in vitro* experiments with a FUS transducer exciting at the same excitation frequency and pressure as for the *in vivo* experiments (Fig. 2). The droplets before vaporization were largely not visible due to the resolution limit, and after droplet vaporization the formed bubbles became apparent in the field of view of the imaging plane. As shown in the images before and after sonication (Fig. 2A–B), OFP droplets vaporized to microbubbles at pressures of 300 kPa and above, while DFB droplets required higher pressures for vaporization (600 kPa and above).

The number of bubbles having been vaporized in the microscope field of view (FOV) were counted for estimating the relative vaporization efficiency. The volume in this FOV was calculated to be 1.69×10^{-8} mL based on a dimension of 130.2 μm × 130.2 μm × 1 μm, which contained 2366 OFP droplets or 1065 DFB droplets assuming homogeneous distribution. For OFP droplets, an average of 11±7 (mean ± standard deviation) bubbles were generated at 300 kPa. This was nearly doubled (25±6 bubbles) when the pressure was increased to 450 kPa. Qualitatively, we observed even more bubbles being generated at even higher pressures (600–900 kPa) for OFP droplets. However, the number of bubbles formed from DFB droplets was lower, although the bubble size could be larger (>10 μm). On

average, 0.4±0.7, 3±2, and 2±1 bubbles were generated at 600, 750, and 900 kPa, respectively. The relative vaporization efficiency (Fig. 2C) was found to be higher for OFP droplets at low pressures than for DFB droplets at high pressures based on the number of bubbles formed in the optical FOV after vaporization and compensated for the nanodroplet concentration. The absolute transition efficiencies were estimated to be 0.5%, 1%, and 0.3% for OFP droplets at 300 kPa, 450 kPa and DFB droplets at 750–900 kPa, respectively.

Through *in vitro* experimentation, it was confirmed that at least six times more microbubbles were generated from OFP droplets compared to DFB droplets when using the same dilution factor (50% dilution with saline). OFP droplets were deemed more efficient acoustic agents with higher vaporization efficiency. We therefore hypothesized that a lower dose of OFP droplets (1/4 volume of the DFB droplets) would be sufficient for the *in vivo* experiments compared to DFB droplets. The estimated droplet concentration in the blood stream was calculated to be 4.7×10^8 particles/mL and 8.7×10^8 particles/mL for OFP and DFB droplets, respectively, based on 1.5 mL volume of blood in mice weighing 25 g.

3.2 Molecular delivery using 40-kDa dextran

The *in vivo* drug delivery using 40-kDa dextran after BBB opening were quantified with fluorescence imaging comparing the fluorescence enhancement in the sonicated hippocampus to the contralateral region (Fig. 3). With the OFP droplets, successful delivery of 40-kDa dextran was found to be at 300 kPa (75%, 3 out of 4 mice)(Fig. 3A) and 450 kPa (100%, 5 out of 5 mice)(Fig. 3B), but not for the 150 kPa group (0 out of 3 mice). For the DFB droplets, successful delivery was found to be at 900 kPa (100%, 4 out of 4 mice) (Fig. 3C), whereas no delivery was detected at 750 kPa (0 out of 4 mice). The quantitative results showed similar delivery achieved for OFP droplets at 300 kPa and DFB droplets at 900 kPa ($p>0.05$) in both the area of successful delivery (Fig. 3D) and the fluorescence intensity increase (Fig. 3E). Furthermore, we were able to achieve significantly higher dextran delivery (in terms of area and fluorescent intensity increase) with OFP droplets at 450 kPa compared to DFP droplets at 900 kPa. Therefore, using OFP droplets we were able to achieve significantly higher delivery at lower pressures with a lower dosage. Notably, sonication at lower pressure (300 kPa) produced similar results as sonication at a high pressure (900 kPa) using DFB droplets even when a 4 times lower dosage of OFP droplets was used, which corresponded to the *in vitro* vaporization efficiency measurement.

3.4 Acoustic cavitation emission

Transcranial cavitation monitoring was performed in all experiments in order to investigate the behavior of cavitation after droplet vaporization associated with drug delivery and bioeffects. The overall cavitation dose representing the accumulative cavitation intensity for each sonication was calculated and shown in Fig. 4. For the OFP droplets, the SCD_h was significantly higher at pressures with successful dextran delivery compared to the control without acoustic agents, showing significant bubble activities occurred after vaporization. Significant SCD_u appeared only at the pressure causing the highest amount of delivery (450 kPa), and no significance was found in the ICD. For DFB droplets, although the SCD_h was insignificant due to the low volumetric bubble oscillation at high pressures, the SCD_u and the ICD showed statistical significance at 900 kPa with successful delivery. Since both types

of the stable cavitation dose was detectable for OFP droplets, their sum ($SCD_{h+u} = SCD_h + SCD_u$) was then plotted against the area of BBB opening (Fig. 4D) as well as the fluorescence intensity increase representing the delivery efficiency (Fig. 4E). In both of them, good agreement ($R^2 = 0.74$, 0.92 for BBB opening area and fluorescence intensity, respectively) was found in cases of successful delivery.

3.5 Bioeffects

The histological (H&E) staining was performed in the cohorts with successful delivery (3 mice from each group: OFP at 300 kPa, OFP at 450 kPa, DFB at 900 kPa) in order to assess any potential tissue damage 1 h after sonication using nanodroplets (Fig. 5). The results showed no damage, i.e., no red blood cell extravasations or dark neurons using OFP droplets at the pressures leading to successful delivery (Fig. 5A–D). These results demonstrate that effective drug delivery for relatively large molecules is possible using OFP droplets, without bioeffects. For DFB droplets at 900 kPa, 2 out of 3 animals showed no damage while 1 had more dark neurons in the sonicated hippocampus (Fig. 5E–F), which may correspond to the statistically significant inertial cavitation detected during sonication (Fig. 4C). Although data regarding the lack of cavitation induced bioeffects during OFP mediated dextran delivery were encouraging, our study was not powered to draw statistical comparisons between the absence or presence of bioeffects during drug delivery with OFP and DFP droplets. A larger study will be performed in the future to provide a more thorough safety assessment of our BBB opening methods (i.e. investigating damage at more time points post-sonication) and to provide a statistical comparison between damage caused using OFP at 300 kPa or 450 kPa compared to DFB at higher pressure (900 kPa).

3.6 Comparing with precursor microbubbles

The in vivo drug delivery experiment was performed using precursor microbubbles at 450 kPa as a comparison to the OFP droplets at 450 kPa, and the results of drug delivery and cavitation monitoring were shown in Fig. 6. The quantified enhanced delivery area and the fluorescence intensity increase was 78.3% and 1.6×10^6 A.U., respectively. The delivery outcomes using OFP droplets were comparable to using microbubbles. Although the enhanced area using OFP droplets was slightly smaller, it was statistically insignificant. For the cavitation monitoring, both the SCD_h and SCD_u were detected as using OFP droplets. The SCD_u were at the same level or even slightly lower, while the SCD_h for microbubbles was much higher.

4. Discussion

Nanodroplets in principle are promising for highly targeted delivery of large molecules to the brain, however, the delivery to the brain is not as effective with DFB droplets as with microbubbles for the same acoustic pressure (Chen *et al.*, 2013a). Here we showed for the first time that delivery of a large amount of molecules as large as proteins is feasible by modulating the droplet vaporization efficiency. OFP droplets are characterized by high vaporization efficiency even at low acoustic pressures due to the low gas boiling points, and could deliver higher amounts of large molecules to the brain without inducing bioeffects assessed with histology. They may be less likely to induce bioeffects compared to DFB

droplets as they can be vaporized and cavitate stably at lower pressures using a lower dosage. The good correlation (R^2=0.92, 0.74) between delivery outcomes and the cavitation dose indicate that the localized drug delivery may be predictable through acoustic cavitation monitoring.

The *in vitro* experiments provided a way to quantify the vaporization threshold and relative vaporization efficiency of droplets, which showed a more than six times higher vaporization efficiency of OFP droplets at 450 kPa compared with DFB droplets at 750–900 kPa. In the experiments, the generated bubbles were assumed to stay in the imaging plane because of the high frame rate used to capture the vaporization events. This assumption was reasonable based on the consistency of the number of bubbles counted at every experiment. In addition, there were two major differences between the in vitro and in vivo study. First, the droplet concentration was higher in the in vitro study in order to capture vaporization events within the narrow field of view in the microscope. Second, shorter pulses were used in the in vitro study in order to visualize the vaporization events and estimate the vaporization threshold without interference by the bubble oscillation and motion. It is difficult to capture vaporization events with very high number of cycles, as generated microbubbles are rapidly pushed out of the field of view and/or destroyed with high cycle numbers.

Moreover, the absolute transition efficiencies (0.3% to 1%) measured in vitro were considered low owing to three reasons. First, only vaporization in the imaging plane were visualized and the off-plane events were not included. Second, at the moderate pressure of 300–450 kPa in this study, only a subset of droplets may be vaporized. Third, the presence of inseparable empty vesicles in the solution such as micelles and liposomes around 100 nm in diameter may increase the droplets concentration. Lastly, DFB droplets tend to vaporize into larger bubbles (> 10 μm) may be due to larger droplet size compared with OFP droplets as shown in Fig. 1. This high expansion ratio could be due to secondary Bjerknes forces causing bubble coalescence after vaporization and/or influx of gases dissolved in the surrounding media into the generated bubbles (Sheeran *et al.*, 2011a). Future *in vitro* experiments will be aimed at characterizing the appearance of these large bubbles in greater detail by analyzing relative bubble motion due to Bjerknes forces (to confirm the tendency for bubbles to coalesce) and/or monitor bubble growth due to influx of gasses.

The *in vivo* drug delivery outcomes using dextrans (Fig. 3) were found to associate with the *in vitro* vaporization efficiency (Fig. 2). For OFP droplets, the pressure threshold for successful drug delivery was the same as the vaporization threshold (300 kPa), and the drug delivery outcomes trended with vaporization efficiency. For DFB droplets, the low number of bubbles formed resulted in no or low delivery at 600–750 kPa. The pressure threshold for successful drug delivery (900 kPa) was higher than the vaporization threshold (600 kPa) due to the difficulty in delivering large molecules with fewer bubbles. The high vaporization efficiency of OFP droplets allowed for drug delivery outcomes comparable to that provided by microbubbles, and could be due to the same amount of gas volume been generated and sonicated in the focal region (Song et al., 2017).

The droplet vaporization efficiency or the ease of droplet vaporization could be tailored through not only the PFC core (Sheeran *et al.*, 2012) but also the lipid chain length of the

shell (Mountford *et al.*, 2015) as well as the droplet size, which modulates the number of droplets being vaporized into microbubbles after applying ultrasound and thus the *in vivo* drug delivery outcome. After microbubble condensation at high pressures, the pure, superheated liquid core of the nanodroplets remain metastable and therefore resists homogeneous nucleation (Mountford *et al.*, 2015). This metastability is determined by the vaporization energy related to the boiling point of the droplet core (Sheeran *et al.*, 2012) and the lipid inter-chain cohesion in the shell (Mountford *et al.*, 2015). In this study through tailoring the boiling point of the PFC core, the low-boiling-point OFP droplets vaporized efficiently to form significantly more bubbles at and above 300 kPa compared to DFB droplets sonicated at 900 kPa. Moreover, the formed OFP bubbles are more stable against dissolution than DFB bubbles based on previous findings (Mountford *et al.*, 2015). Therefore, OFP bubbles once formed could cavitate stably over long pulses and generate shear stress on neighboring endothelial cells for prolonged durations (Doinikov and Bouakaz, 2010). As a result, the OFP droplets could achieve significantly higher amounts of delivery even for large molecules *in vivo* at lower acoustic pressures with 1/4 dosage compared to DFP droplets.

The acoustic emission during BBB opening (Fig. 4) reflected the behavior of cavitation associated with drug delivery and absence of cavitation induced bioeffects after droplet vaporization. A significant stable cavitation dose (SCD_h and SCD_u for volumetric oscillation and/or surface oscillation) was detected in groups with successful delivery, meaning that stable cavitation was effective to achieve drug delivery due to highly localized and strong shear stress applied on the vessel wall after droplet vaporization. Harmonic emission was detected in the cases of the OFP droplets but not for DFB droplets possibly because the bubbles were rapidly disrupted after vaporization at high pressures (e.g. 900 kPa). Nevertheless, ultraharmonics were detected for both OFP and DFB droplets since they were associated with irregular bubble oscillation and may lead to bubble disruption at high pressures. They were also less affected by the nonlinear effect from the skull or tissue generating harmonics. Interestingly, stronger ultraharmonics were found in droplets with 100% successful delivery (OFP droplets at 450 kPa and DFP droplets at 900 kPa) compared to microbubbles. This implied that irregular oscillation with bubbles after nanodroplet vaporization were indicative of increased BBB permeability, and may be due to the fact that larger bubbles formed after droplet vaporization are more compliant and more prone to irregular oscillations and increased shear stress to the vessel walls compared with smaller bubbles (Chen *et al.*, 2013b).

The potential to induce cellular damage can be assessed by inertial cavitation with droplets, similar to what has been reported with microbubbles (Tung *et al.*, 2011). Significant inertial cavitation occurred at 900 kPa for DFB droplets, and we observed damage in one of three mice in our bioeffects assessment. The bubbles were likely disrupted right after droplet vaporization at 900 kPa, and these strong shock waves and microjets may have caused damage (Fig. 5). On the other hand, OFP droplets did not cause any damage (zero of three mice) since the bubbles were mainly undergoing stable cavitation at 300–450 kPa after vaporization, as demonstrated by insignificant broadband emissions (ICD). Therefore, for delivering large molecules, OFP droplets could be safer than DFB droplets due to the OFP vaporization threshold falling in the regime of stable cavitation. Furthermore, from a dosing

perspective, OFP droplets may prove to be a safer alternative to DFP droplets as a lower dose can be used to achieve the same concentration of generated microbubbles as OFP droplets are characterized by higher vaporization efficiency. Moreover, although larger droplets (micron size) have been used for embolization, this microvascular embolism was prevented by using small and low dose of nanodroplets in this study. The ischemic stroke from microvascular embolism could result in neuronal death, and could have been detected by the standardized H&E staining (i.e., dark neurons) if occurred (Zille *et al.*, 2012).

As shown in this study, OFP droplets can enhance drug delivery as significantly as using microbubbles for BBB opening, and good correlation with cavitation occurrence indicates potential for real-time monitoring or control of the treatment. There are three main advantages using OFP droplets for BBB opening and drug delivery compared with using microbubbles. First, nanodroplets may result in a more homogeneous delivery because they may be able to distribute more extensively in vessels and capillaries due to their small size. In contrast, more microbubbles (due to the size) may locate more in larger vessels than in the small and sometime more tortuous capillaries. Second, nanodroplets could be more persistent in the blood stream compared to microbubbles (Sheeran et al., 2015). This characteristic would benefit the applications requiring longer sonication time for higher amount or larger area of delivery. Lastly, the use of nanodroplets could potentially avoid the microbubble shielding effects and increase local deposition of acoustic energy as shown in a previous study (Phillips *et al.*, 2013).

The main restriction to using highly-efficient nanodroplets is spontaneous vaporization due to the highly volatile nature of OFP. This spontaneous vaporization may occur at higher temperatures (> 4 °C) after been thawed, with a quick temperature change such as been taken out from −80 °C freezer to be thawed at room temperature (as compared to being thawed in the 4°C fridge), or even during injection to the bloodstream. Therefore, low OFP droplet concentration should be chosen in order to avoid embolism from spontaneous vaporization upon injection, and injections handled speedily with care because of their lower stability at room temperature (10 min. for OFP droplets vs. 1 h for DFB droplets (Sheeran *et al.*, 2012)). Although spontaneous vaporization was observed in the *in vitro* experiments, its effect on drug delivery in this study was deemed insignificant with the current dosage, as the SCD_h is sensitive especially at lower pressures with microbubbles (Wu *et al.*, 2014; Bader and Holland, 2013; Stride, 2009) but was insignificant with OFP droplets at 150 kPa and remained low at 300 kPa.

Future applications for utilizing nanodroplets for drug delivery to the brain could be based on their smaller size and the ability to encapsulate drugs. Their presence in the brain parenchyma could enhance drug delivery through sonoporation, or facilitate thermal ablation or occlusion therapy for droplets accumulated in tumors or other tissues in the brain. Moreover, nanodroplets could serve as drug carrier for targeted delivery and possibly achieve more effective drug delivery due to the higher drug payload in the liquid core. On the other hand, the nanodroplets could possibly enter the parenchyma through intranasal delivery (Chen *et al.*, 2014).

5. Conclusion

Aiming to enhance drug delivery to the brain, nanodroplets of different vaporization efficiencies were characterized and utilized with focused ultrasound to open the BBB for molecular delivery. The findings showed that drug delivery outcomes could be associated with the relative vaporization efficiency, i.e., the relative number of bubbles formed after vaporization. Furthermore, the delivery with OFP nanodroplets was comparable to using microbubbles. We expect OFP droplets to be a safer alternative to DFB droplets due to the lower vaporization threshold and lower dosage used. Our results constitute the first *in vivo* demonstration of BBB opening using lower-boiling point OFP nanodroplets for delivering significant amount of large molecules to the brain, via modulating the vaporization efficiency to improve delivery outcomes.

Supplementary Material

Refer to Web version on PubMed Central for supplementary material.

Acknowledgments

This study was supported in part by National Institutes of Health R21 EB021103, R01 AG038961, R01 EB009041 to E.E.K., and K12 GM000678 to C.B.A. The authors wish to thank Paul Sheeran (PhD, University of North Carolina) and Hong Chen (PhD, Columbia University) for their input and insightful discussions. P.A.D. is an inventor on a patent describing low-boiling point nanodroplet technology.

References

Bader KB, Holland CK. Gauging the likelihood of stable cavitation from ultrasound contrast agents. Phys Med Biol. 2013; 58:127–44. [PubMed: 23221109]

Banks WA. From blood-brain barrier to blood-brain interface: new opportunities for CNS drug delivery. Nat Rev Drug Discov. 2016; 15:275–92. [PubMed: 26794270]

Baseri B, Choi JJ, Deffieux T, Samiotaki G, Tung YS, Olumolade O, Small SA, Morrison B, Konofagou EE. Activation of signaling pathways following localized delivery of systemically administered neurotrophic factors across the blood-brain barrier using focused ultrasound and microbubbles. Phys Med Biol. 2012; 57:N65–81. [PubMed: 22407323]

Baseri B, Choi JJ, Tung YS, Konofagou EE. Multi-Modality Safety Assessment of Blood-Brain Barrier Opening Using Focused Ultrasound and Definity Microbubbles: A Short-Term Study. Ultrasound Med Biol. 2010; 36:1445–59. [PubMed: 20800172]

Chen CC, Sheeran PS, Wu SY, Olumolade OO, Dayton PA, Konofagou EE. Targeted drug delivery with focused ultrasound-induced blood-brain barrier opening using acoustically-activated nanodroplets. J Control Release. 2013a; 172:795–804. [PubMed: 24096019]

Chen CC, Wu S-Y, Finan JD, Morrison B, Konofagou E. An experimental study on the stiffness of size-isolated microbubbles using atomic force microscopy. IEEE Trans Ultrason Ferroelectr Freq Control. 2013b; 60:524–34. [PubMed: 23475918]

Chen H, Chen CC, Acosta C, Wu SY, Sun T, Konofagou EE. A new brain drug delivery strategy: focused ultrasound-enhanced intranasal drug delivery. PLoS ONE. 2014; 9:e108880. [PubMed: 25279463]

Chen H, Konofagou EE. The size of blood-brain barrier opening induced by focused ultrasound is dictated by the acoustic pressure. J Cereb Blood Flow Metab. 2014; 34:1197–204. [PubMed: 24780905]

Choi JJ, Pernot M, Small SA, Konofagou EE. Noninvasive, transcranial and localized opening of the blood-brain barrier using focused ultrasound in mice. Ultrasound Med Biol. 2007; 33:95–104. [PubMed: 17189051]

Choi JJ, Wang S, Tung YS, Morrison B 3rd, Konofagou EE. Molecules of various pharmacologically-relevant sizes can cross the ultrasound-induced blood-brain barrier opening in vivo. Ultrasound Med Biol. 2010; 36:58–67. [PubMed: 19900750]

Davies ER. A Modified Hough Scheme for General Circle Location. Pattern Recogn Lett. 1988; 7:37–43.

Dayton PA, Zhao S, Bloch SH, Schumann P, Penrose K, Matsunaga TO, Zutshi R, Doinikov A, Ferrara KW. Application of ultrasound to selectively localize nanodroplets for targeted imaging and therapy. Mol Imaging. 2006; 5:160–74. [PubMed: 16954031]

Doinikov AA, Bouakaz A. Theoretical investigation of shear stress generated by a contrast microbubble on the cell membrane as a mechanism for sonoporation. J Acoust Soc Am. 2010; 128:11–9. [PubMed: 20649196]

Kinoshita M, McDannold N, Jolesz FA, Hynynen K. Noninvasive localized delivery of Herceptin to the mouse brain by MRI-guided focused ultrasound-induced blood-brain barrier disruption. Proc Natl Acad Sci U S A. 2006a; 103:11719–23. [PubMed: 16868082]

Kinoshita M, McDannold N, Jolesz FA, Hynynen K. Targeted delivery of antibodies through the blood-brain barrier by MRI-guided focused ultrasound. Biochem Biophys Res Commun. 2006b; 340:1085–90. [PubMed: 16403441]

Konofagou E E. Optimization of the ultrasound-induced blood-brain barrier opening. Theranostics. 2012; 2:1223–37. [PubMed: 23382778]

Kopechek JA, Park EJ, Zhang YZ, Vykhodtseva NI, McDannold NJ, Porter TM. Cavitation-enhanced MR-guided focused ultrasound ablation of rabbit tumors in vivo using phase shift nanoemulsions. Physics in Medicine and Biology. 2014; 59:3465–81. [PubMed: 24899634]

Kripfgans OD, Fowlkes JB, Miller DL, Eldevik OP, Carson PL. Acoustic droplet vaporization for therapeutic and diagnostic applications. Ultrasound Med Biol. 2000; 26:1177–89. [PubMed: 11053753]

Kripfgans OD, Fowlkes JB, Woydt M, Eldevik OP, Carson PL. In vivo droplet vaporization for occlusion therapy and phase aberration correction. IEEE Trans Ultrason Ferroelectr Freq Control. 2002; 49:726–38. [PubMed: 12075966]

Leinenga G, Langton C, Nisbet R, Gotz J. Ultrasound treatment of neurological diseases - current and emerging applications. Nat Rev Neurol. 2016; 12:161–74. [PubMed: 26891768]

Li HW, Lavin MA, Lemaster RJ. Fast Hough Transform - a Hierarchical Approach. Comput Vision Graph. 1986; 36:139–61.

Liu HL, Fan CH, Ting CY, Yeh CK. Combining microbubbles and ultrasound for drug delivery to brain tumors: current progress and overview. Theranostics. 2014; 4:432–44. [PubMed: 24578726]

Liu HL, Hsu PH, Lin CY, Huang CW, Chai WY, Chu PC, Huang CY, Chen PY, Yang LY, Kuo JS, Wei KC. Focused Ultrasound Enhances Central Nervous System Delivery of Bevacizumab for Malignant Glioma Treatment. Radiology. 2016a; 281:99–108. [PubMed: 27192459]

Liu WW, Liu SW, Liou YR, Wu YH, Yang YC, Wang CR, Li PC. Nanodroplet-Vaporization-Assisted Sonoporation for Highly Effective Delivery of Photothermal Treatment. Sci Rep. 2016b; 6:24753. [PubMed: 27094209]

Marquet F, Tung YS, Teichert T, Ferrera VP, Konofagou EE. Noninvasive, transient and selective blood-brain barrier opening in non-human primates in vivo. PLoS ONE. 2011; 6:e22598. [PubMed: 21799913]

Matsunaga TO, Sheeran PS, Luois S, Streeter JE, Mullin LB, Banerjee B, Dayton PA. Phase-change nanoparticles using highly volatile perfluorocarbons: toward a platform for extravascular ultrasound imaging. Theranostics. 2012; 2:1185–98. [PubMed: 23382775]

Mountford PA, Thomas AN, Borden MA. Thermal activation of superheated lipid-coated perfluorocarbon drops. Langmuir. 2015; 31:4627–34. [PubMed: 25853278]

Moyer LC, Timbie KF, Sheeran PS, Price RJ, Miller GW, Dayton PA. High-intensity focused ultrasound ablation enhancement in vivo via phase-shift nanodroplets compared to microbubbles. J Ther Ultrasound. 2015; 3:7. [PubMed: 26045964]

Phillips LC, Puett C, Sheeran PS, Wilson Miller G, Matsunaga TO, Dayton PA. Phase-shift perfluorocarbon agents enhance high intensity focused ultrasound thermal delivery with reduced near-field heating. J Acoust Soc Am. 2013; 134:1473–82. [PubMed: 23927187]

Porter TR, Arena C, Sayyed S, Lof J, High RR, Xie F, Dayton PA. Targeted Transthoracic Acoustic Activation of Systemically Administered Nanodroplets to Detect Myocardial Perfusion Abnormalities. Circ Cardiovasc Imaging. 2016; 9

Rapoport N, Nam KH, Gupta R, Gao Z, Mohan P, Payne A, Todd N, Liu X, Kim T, Shea J, Scaife C, Parker DL, Jeong EK, Kennedy AM. Ultrasound-mediated tumor imaging and nanotherapy using drug loaded, block copolymer stabilized perfluorocarbon nanoemulsions. J Control Release. 2011; 153:4–15. [PubMed: 21277919]

Samuel S, Duprey A, Fabiilli ML, Bull JL, Fowlkes JB. In vivo microscopy of targeted vessel occlusion employing acoustic droplet vaporization. Microcirculation. 2012; 19:501–9. [PubMed: 22404846]

Sheeran PS, Luois S, Dayton PA, Matsunaga TO. Formulation and acoustic studies of a new phase-shift agent for diagnostic and therapeutic ultrasound. Langmuir. 2011a; 27:10412–20. [PubMed: 21744860]

Sheeran PS, Luois SH, Mullin LB, Matsunaga TO, Dayton PA. Design of ultrasonically-activatable nanoparticles using low boiling point perfluorocarbons. Biomaterials. 2012; 33:3262–9. [PubMed: 22289265]

Sheeran PS, Rojas JD, Puett C, Hjelmquist J, Arena CB, Dayton PA. Contrast-enhanced ultrasound imaging and in vivo circulatory kinetics with low-boiling-point nanoscale phase-change perfluorocarbon agents. Ultrasound Med Biol. 2015; 41:814–31. [PubMed: 25619781]

Sheeran PS, Wong VP, Luois S, McFarland RJ, Ross WD, Feingold S, Matsunaga TO, Dayton PA. Decafluorobutane as a phase-change contrast agent for low-energy extravascular ultrasonic imaging. Ultrasound Med Biol. 2011b; 37:1518–30. [PubMed: 21775049]

Song K-H, Fan AC, Hinkle JJ, Newman J, Borden M, Harvey BK. Microbubble gas volume: a unifying dose parameter in blood-brain barrier opening by focused ultrasound. Theranostics. 2017; 7

Stride E. Physical principles of microbubbles for ultrasound imaging and therapy. Cerebrovascular diseases (Basel, Switzerland). 2009; 27(Suppl 2):1–13.

Timbie KF, Mead BP, Price RJ. Drug and gene delivery across the blood-brain barrier with focused ultrasound. J Control Release. 2015

Tung YS, Vlachos F, Feshitan JA, Borden MA, Konofagou EE. The mechanism of interaction between focused ultrasound and microbubbles in blood-brain barrier opening in mice. J Acoust Soc Am. 2011; 130:3059–67. [PubMed: 22087933]

Wang CH, Kang ST, Yeh CK. Superparamagnetic iron oxide and drug complex-embedded acoustic droplets for ultrasound targeted theranosis. Biomaterials. 2013; 34:1852–61. [PubMed: 23219326]

Wu S-Y, Sanchez CS, Samiotaki G, Buch A, Ferrera V, Konofagou E. Characterizing Focused-Ultrasound Mediated Drug Delivery to the Heterogeneous Primate Brain In Vivo with Acoustic Monitoring. Sci Rep. 2016; 6

Wu SY, Chen CC, Tung YS, Olumolade OO, Konofagou EE. Effects of the microbubble shell physicochemical properties on ultrasound-mediated drug delivery to the brain. J Control Release. 2015; 212:30–40. [PubMed: 26065734]

Wu SY, Tung YS, Marquet F, Downs M, Sanchez C, Chen C, Ferrera V, Konofagou E. Transcranial cavitation detection in primates during blood-brain barrier opening--a performance assessment study. IEEE Trans Ultrason Ferroelectr Freq Control. 2014; 61:966–78. [PubMed: 24859660]

Zhou Y. Application of acoustic droplet vaporization in ultrasound therapy. J Ther Ultrasound. 2015; 3:20. [PubMed: 26566442]

Zille M, Farr TD, Przesdzing I, Muller J, Sommer C, Dirnagl U, Wunder A. Visualizing cell death in experimental focal cerebral ischemia: promises, problems, and perspectives. J Cereb Blood Flow Metab. 2012; 32:213–31. [PubMed: 22086195]

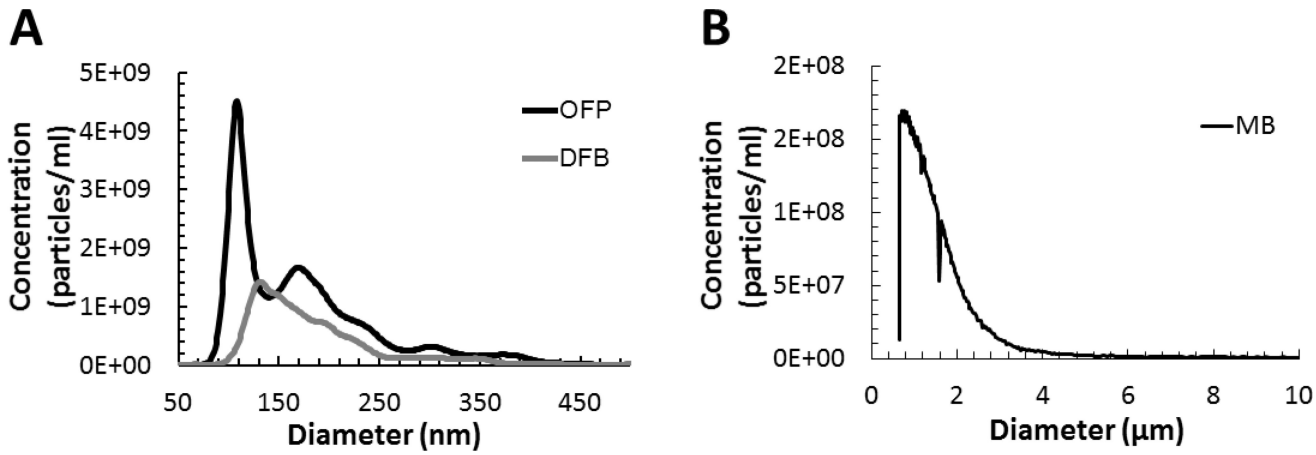

Figure 1.

The average size distribution of (A) the droplet emulsions and (B) the precursor microbubbles. The average concentration and the median size for OFP droplets were 2.8×10^{11} particles/mL and 171 nm, respectively; those for DFP droplets were 1.3×10^{11} particles/mL and 183 nm, respectively; those for microbubbles were 1.5×10^{10} particles/mL and 1.1 μm.

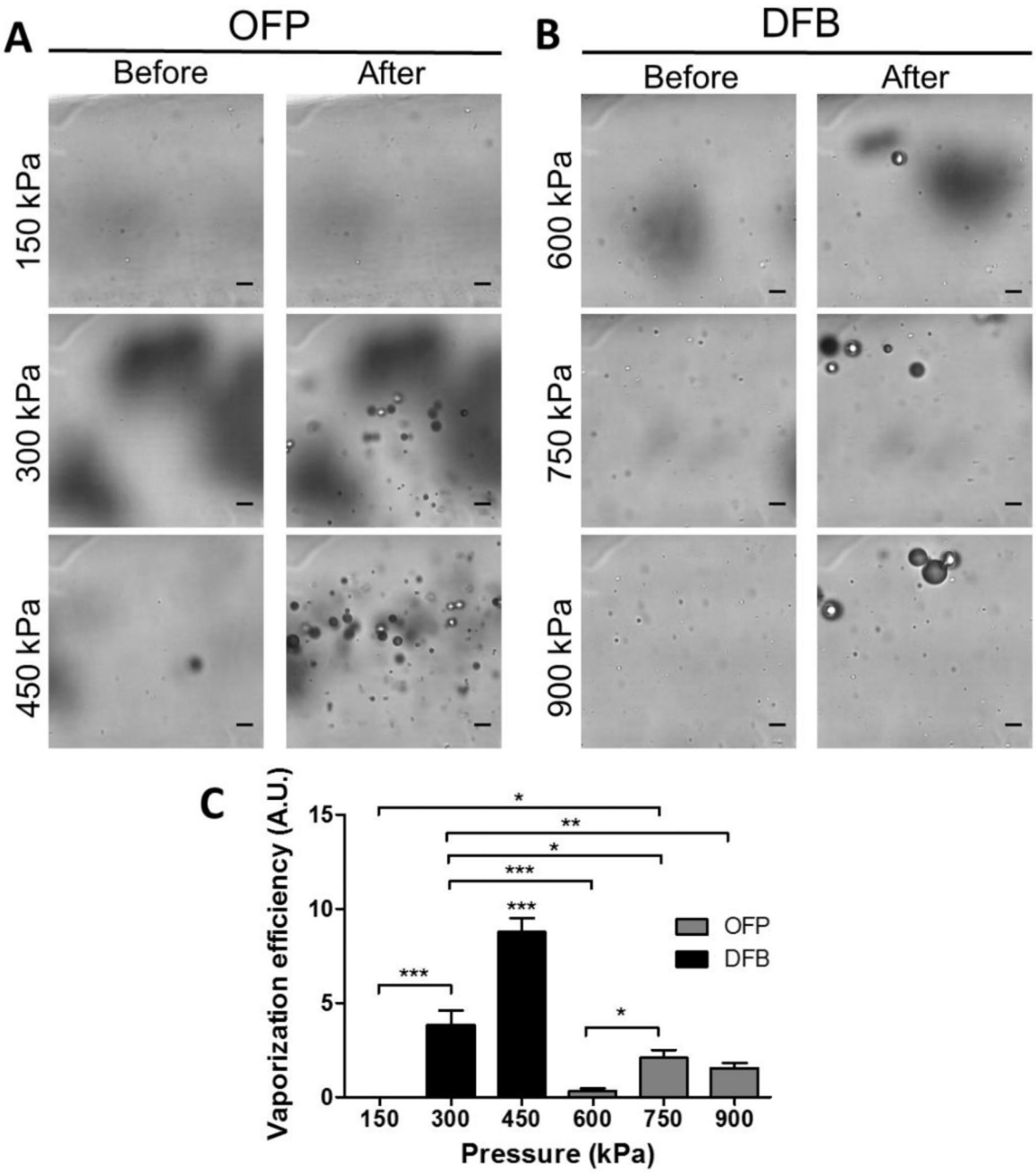

Figure 2.

Detection of acoustic droplet vaporization using high-speed optical microscopy (0 and 6 ms after sonication). (A) OFP-filled droplets were found to vaporize at pressures at and above 300 kPa, but not at 150 kPa. (B) DFB droplets were found to vaporize inconsistently at 600 kPa (vaporization did not occur with every activation pulse). Vaporization was consistently observed at 750 kPa and 900 kPa for DFB droplets. On average, more bubbles were generated from OFP droplets at low pressures (300–450 kPa) compared to those generated from DFB droplets at higher pressures (750–900 kPa). Scale bar represents 10 μm. (C) The relative vaporization efficiency was calculated by dividing the number of bubbles formed in

the field of view by the nanodroplets concentration (10^{11} droplets/mL) measured with NanoSight. The vaporization efficiency of OFP droplets was higher than that of DFB droplets. Note that *** in (C) on top of OFP droplets at 450 kPa represents the same level of statistical significant to all the other cohorts.

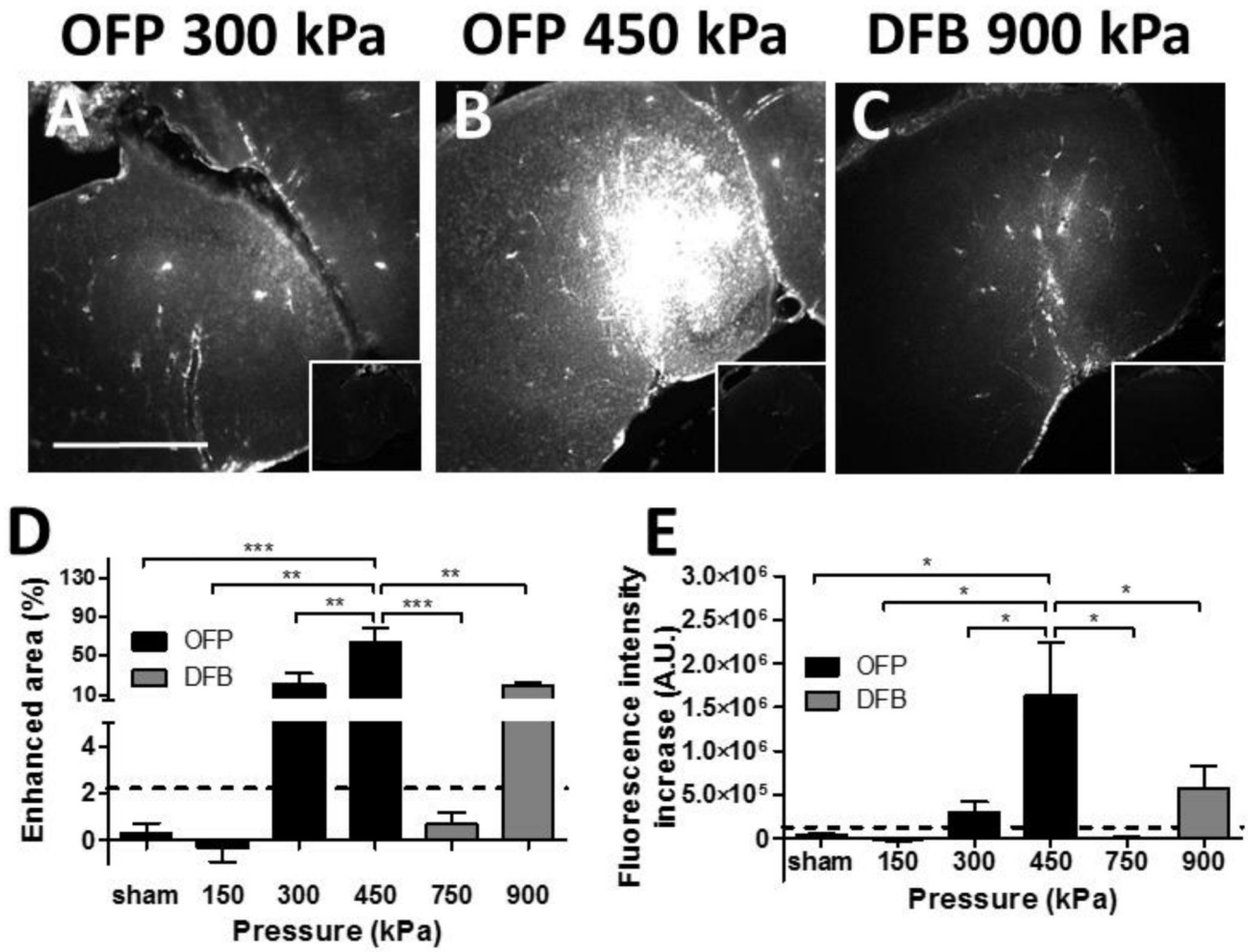

Figure 3.

Delivery efficiency of 40-kDa dextran using fluorescence microscopy after BBB opening. Fluorescence images of sonicated vs. non-sonicated hippocampi (insets) using (A) OFP droplets at 300 kPa, (B) OFP droplets at 450 kPa, (C) DFB droplets at 900 kPa. (D) The average enhanced area due to successful delivery (normalized to the entire hippocampus) and (E) average fluorescence intensity increase for all cohorts, with a dash line representing the threshold of successful delivery defined by the sham group (mean plus 2 time of the standard deviation). Successful delivery was found to be at and above 300 kPa for OFP droplets, and 900 kPa for DFB droplets. Note that OFP represents OFP droplets and DFB for DFB droplets. The scale bar in (A) represents 1 mm.

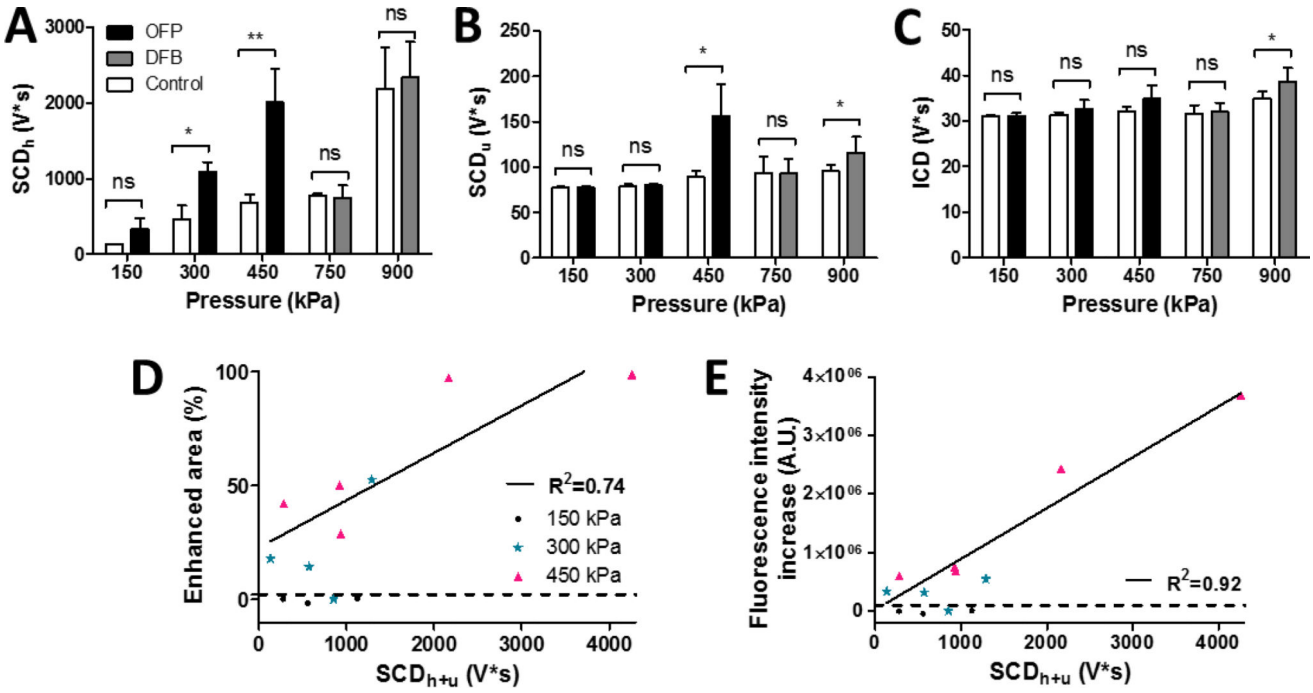

Figure 4.

Cavitation dose of the entire sonication. (A) SCD_h or stable cavitation dose with harmonic emissions. (B) SCD_u or stable cavitation dose with ultraharmonic emissions. (C) ICD or inertial cavitation dose with broadband emissions. (D) The area of successful delivery and (E) the fluorescence intensity increase using OFP droplets was linearly correlated with the total stable cavitation dose ($SCD_{u+h} = SCD_h + SCD_u$) for the cases with successful delivery. The dash line represents the threshold of successful delivery defined by the sham group (mean plus two times of the standard deviation).

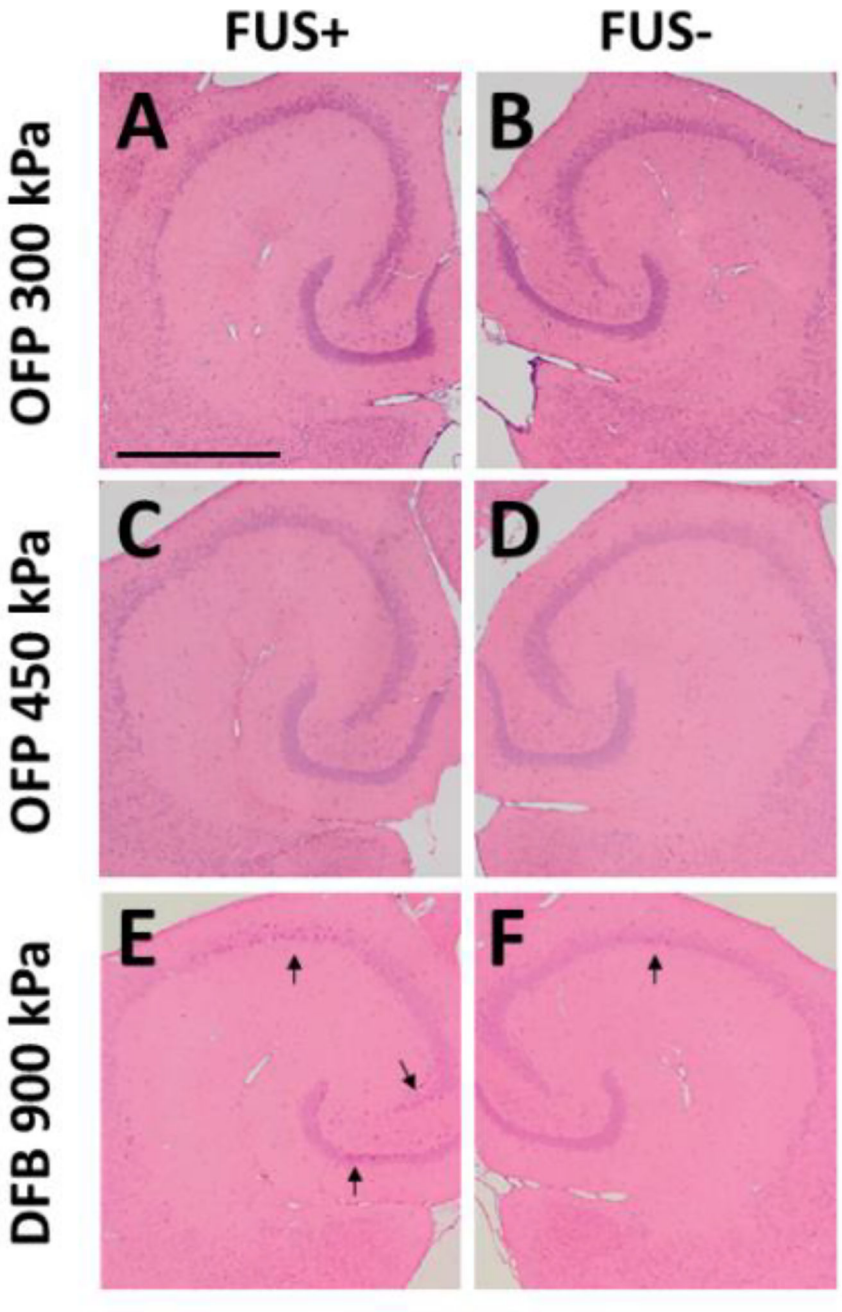

Figure 5.

Bioeffect assessment using histological staining (H&E). Sonicated (A, C, E) and nonsonicated (B, D, F) hippocampi using OFB at 300 kPa (A, B), 450 kPa (C, D), and DFB at 900 kPa (E, F). The results showed no damage (erythrocyte extravasations or dark neurons) using OFP droplets. For DFB droplets at 900 kPa, only 1 out of 3 animals showed an increased number of dark neurons on the hippocampi. The scale bar in (A) represents 1 mm.

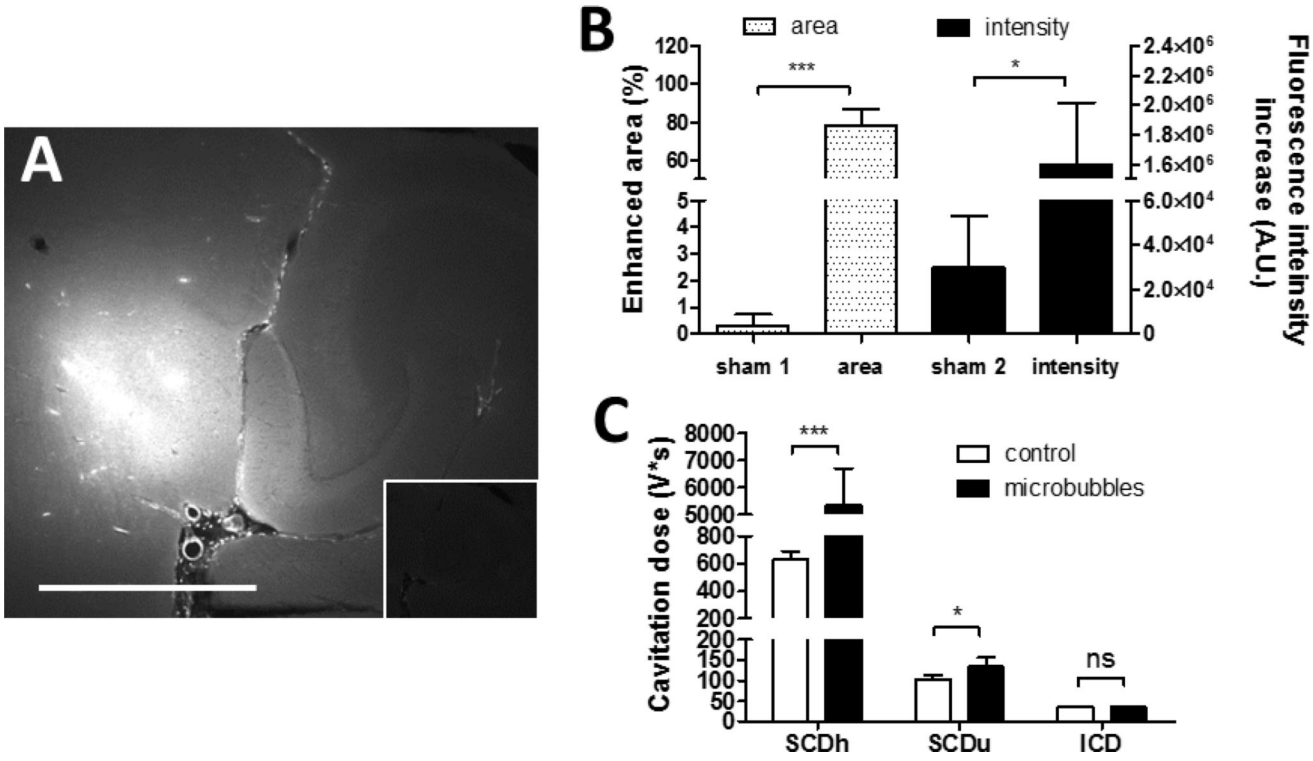

Figure 6.

40-kDa dextran delivery and cavitation detection using microbubbles at 450 kPa. (A) Fluorescence images of sonicated vs. non-sonicated hippocampi (insets). The scale bar represents 1 mm. (B) The average enhanced area due to successful delivery (normalized to the entire hippocampus) and the average fluorescence intensity. (C) Cavitation dose of the entire sonication.

Table 1

Number of animals in each experimental cohort.

Group	Acoustic agents	Number of mice per experimental condition					
		Sham	Acoustic pressure (kPa)				
			150	300	450	750	900
1	OFP droplets	4	3	7*	8*	-	-
2	DFB droplets	-	-	-	-	4	7*
3	Microbubbles	-	-	-	5	-	-

* Number shown including 3 mice per experimental condition used for histological examination.

Phys Med Biol. Author manuscript; available in PMC 2019 January 22.